

Virtual Manufacturing for Prediction of Martensite Formation and Hardness Value induced by Laser Welding Process using Subroutine Algorithm in MSC Marc/Mentat

*Omar Yahya, Yupiter HP Manurung, Mohd Shahar Sulaiman, Keval P Prajadhiana, Abdul Rahman Omar and Wahyu Kuntjoro
Faculty of Mechanical Engineering, UiTM Shah Alam*

*Henning van Werde
Faculty of Engineering and Computer Science,
University of Applied Sciences Osnabrueck, Germany*

*Alexander Bauer and Marcel Graf
Professorship of Virtual Production Engineering, Chemnitz University of
Technology, Germany*

*Corresponding e-Mail:
yupiter.manurung@salam.uitm.edu.my*

ABSTRACT

In this paper, a coupled thermal-structural and metallurgical model of laser welding process is simulated by using Finite Element Method (FEM) enhanced with Fortran-based subroutine within MSC Marc/Mentat. The investigated model specimen is in the form of butt joint plate with thickness of 2mm and material of low carbon steel (C15). The core purpose of the simulation is to predict Martensite formation and hardness value after laser welding process. In the simulation, a heat source model following conical shape is implemented instead of existing Goldak's double ellipsoid used commonly for arc welding process. The Martensite formation and hardness are predicted based on Syyfarth-Kassatkin Model, the results of which are to be verified with the welding Continuous Cooling Transformation (CCT) diagram. It can be concluded that the algorithms to model the heat source

and to calculate the cooling time $t_{8/5}$ are successfully developed and implemented. The simulated heat source shape produced using conical model represents good similar feature with typical laser heat source. Based on the calculated $t_{8/5}$, it is also found that the results of Martensite formation and hardness value show good agreement within acceptable discrepancy compared to the approximated analysis from CCT diagram.

Keywords: Finite Element Method, Welding Simulation, Heat Source Model, Martensite Formation, Hardness, $t_{8/5}$

Introduction

Welding is one of the most common and reliable joining method used in most manufacturing industry. The welding process joins materials by causing coalescence between parent material and the filler material [1]. This is done by introducing heat, by means such as an electric arc or a laser beam, to melt the work piece and adding a filler material. A welding simulation is implemented to predict the outcome of a welding process. It is a common practice in manufacturing, especially in the automobile industry, which helps to reduce the cost of experimentation and to determine the effects of the welding parameters such as voltage, current, weld speed and sequence. By applying simulation, economic benefits could be gained by reducing the amount of rework and scraps due to defects and unwanted properties.

In a welding simulation using FEM, an important factor to be considered is the heat source model. The Goldak double ellipsoid model is mostly used as the heat source model in a typical simulation of an arc welding process. This is due to its accuracy and reliability in representing the shape and distribution of the heat flux [2]. However, in other welding process such as the laser welding process, the Goldak model could no longer accurately represent the actual heat source [3]. The double ellipsoid shaped Goldak model differs vastly with the conical shaped laser heat source. In the latest version MSC Marc/Mentat, a cylindrical model could be used to represent the laser beam. While the model might be sufficient for most application, it does not accurately represent the laser heat source. Since the shape of the heat source will influence the temperature distribution in the plate, a new heat source model must first be developed in order to accurately simulate a laser welding process. The conical heat source model is developed and implemented with the use of a user defined subroutine that will replace both the double ellipsoid and cylindrical model in MSC Marc/Mentat software. Unlike the cylindrical model, the conical model takes into account the varying intensity of the heat flux, whereby the intensity of the heat flux is higher at the centre of the cone and also decreases in intensity with the depth.

Since the welding process is a high temperature process, it has many thermal induced side effects such as change in microstructure. Metallurgical change is a critical factor that needs to be considered in any welding process as the resulting microstructure will define the mechanical properties of the weldment and the heat affected zone (HAZ). The most common concern among welding engineers is the formation of martensitic dendrites in the HAZ. The Martensite formation occurs as a result of fast heating and the following rapid cooling [4]. The increased percentage of Martensitic microstructure in the material will alter the mechanical properties of the parent material such as increased brittleness and hardness. In many applications that require the welding process, this phenomenon is usually undesired as it will encourage crack propagation and reduced toughness. Besides that, the microstructure formation also plays a vital role in determining the residual stress caused by the welding process [5]. As such, the Martensite formation prediction is very important to achieve the optimum properties. However, the capability to simulate microstructure and phase changes are not available by default in the MSC Marc/Mentat. As such, there is a need to implement a mathematical model in order to simulate this phenomenon.

The implementation of the model is established by writing user subroutines to be used by the finite element analysis (FEA) software. The model chosen in this project is the Seyffarth Kassatkin (1984) model. Based on this model and the research done by Patrick Mehmert [6], the percentage of Martensite distribution can be calculated and simulated using numerical method. Although several other models for phase transformation exist, such as investigated by Ausitin-Ricket in 1935, Leblond in 1984 and LSG2M in 1994 [7], the Seyffarth-Kassatkin (S-K) model was chosen due to the practicability within MSC Marc/Mentat software. However, the S-K model can only be used to calculate the phase changes for materials within a limited range of chemical composition.

The theory behind the S-K model depends largely on the time taken for the material to cool down from 800 to 500 degrees Celsius or also known as the $t_{8/5}$. The $t_{8/5}$ concept is a widely used concept in the welding industry to predict and control phase changes during the welding process. Several other studies have been done using the $t_{8/5}$ approach with other phase transformation models [8]. Using the $t_{8/5}$, it is also possible to calculate the resulting hardness value of the material after the welding process.

Simulation Procedure of Laser Welding using Nonlinear FEM

Weld Modelling and Simulation using MSC Marc/Mentat

The thermo-mechanical simulation of the welding process is applied using MSC MSC Marc/Mentat. The simulation is divided into 3 stages; pre-

processing, solving and post-processing. The general flow of the simulation is displayed in the flow chart below, where the first seven stages are pre-processing followed by solving and post processing.

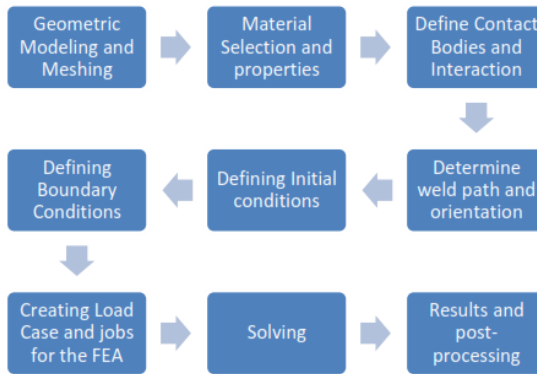


Figure 1: General Flowchart of simulation procedure using MSC Marc/Mentat

Geometrical and Material Description

The modelling of each plates is done using MSC Mentat itself, with dimension of 50 mm in length 25 mm in width and 2 mm in thickness. Figure 2 below illustrates the schematic drawing of the plates and also the modelled plates with quad-meshing.

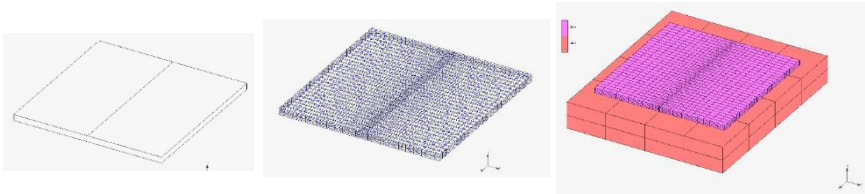


Figure 2: 3D modelling of the plates (left), plates with applied quad-mesh (middle) and complete setup with table (right)

The chosen type of meshing is quad-mesh due to the geometric shape of the work piece to be relatively simplified. Since not much strain and change of shape is expected, using simplified mesh is done to save computing time and ease the modelling effort. A biased meshing is also used to obtain a finer mesh near the centre.

In this simulation, the C15 steel is selected as material for plates. This material is chosen due to its closeness in terms of material composition and

properties with commonly used mild steel. The physical properties of the material are shown in Table 1 below. Some properties of the material are affected at elevated temperature and requires temperature dependent values as shown in Figure 3 below

Table 1: Material Properties of C15

Welding parameters	Value
Young's Modulus (GPa), E	210
Minimum yield strength, γ (MPa)	300
Poisson's ratio, ν	0.3
Density, ρ (kg/m ³)	7850
Melting temperature, t_m (°C)	1540

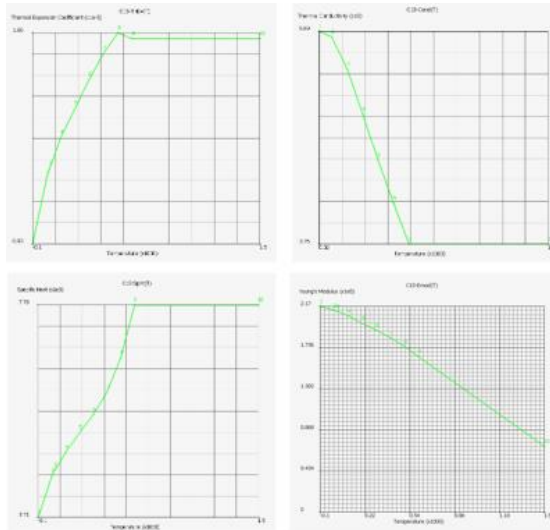


Figure 3: Temperature-dependant thermo-physical properties of C15 (clockwise direction: Thermal Expansion Coefficient, Thermal Conductivity, Young's Modulus and Specific Heat)

Another important consideration is the latent heat properties of the plates. Since the temperature of the plates reach the solidus and comes nears the liquidus line, latent heat properties are defined for the material. This greatly improves the accuracy of the thermal cycle experienced by the plates by preventing the plates reaching excessive temperatures.

Assigning Contact Body and Interaction

All of the bodies in the simulation are defined as a contact body. However, the type of contact body differs. While the plates are defined as deformable bodies, the table is defined as a rigid body. This is done because it is assumed that the table does not undergo any deformation. This not only simplifies the simulation but also save calculation time significantly. All bodies are assumed to be just touching with each other and no parts are glued. By doing so, deformations are allowed as the parts are allowed to move freely from each contact bodies.

Welding path and orientation

The weld path is defined using nodes located in the middle of the weldment. The orientation is defined to be perpendicular to the surface of the plates. The figure below illustrates the weld path and orientation where the weld path is represented by the blue arrow and the weld direction (root) is represented with the green arrow.

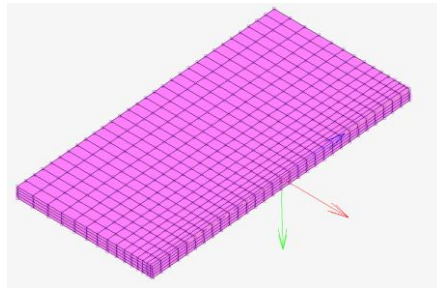


Figure 4: Weld path and orientation.

Initial and Boundary Conditions

For this simulation, only a thermal initial condition is defined. The elements of the plates and table is defined to be at room temperature of 30° Celsius. For the boundary condition, both thermal and structural boundary condition is applied. To simulate the cooling effects of the environment, a film boundary condition is applied to the surface of the plates. This boundary condition is used to consider the effects of heat loss through radiation and convection. The ambient temperature of the environment is defined to be at 30° Celsius. Heat loss due to contact with the table is also considered by applying a contact heat transfer coefficient of 1000 W/m²K while the film coefficient is defined at 25 W/m²K.

Four point-loads are also applied to the nodes on the plate to represent the clamping force. The location and direction of the force applied is shown in Figure 5 below.

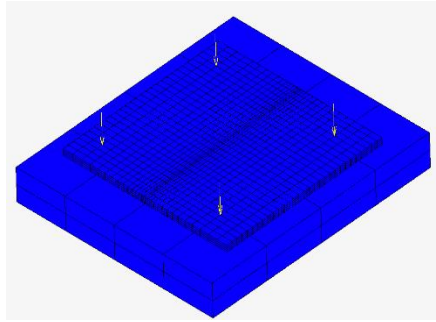


Figure 5: Clamping position of structural boundary condition

A thermal boundary condition, volume weld flux is applied to simulate the welding process on the plate. The welding parameters are displayed in Table 2 below.

Table 2 : Welding parameters used in Simulation

Welding Parameter	Value
Power (W)	700
Travel Speed, v (mm/s)	7

By default, the Goldak double ellipsoid heat source model is defined in the boundary condition. However, to simulate the effects of a laser welding process, the Goldak model is replaced using a user defined subroutine *UWELDFLUX* to implement a conical heat source.

Load case and jobs

A load case is created where all loads and boundary condition is applied. The simulation time is defined to be 60 seconds with a constant time step of 0.1 second per increment. The total increment of 600 could be increased to achieve a more detailed simulation, however this would drastically increase calculation time.

Post-Processing

Before the job is submitted to the FEA another subroutine is included to enable the calculation of phase transformation. This is done by including a post processing subroutine named *PLOTV* and utility routine *ELMVAR* to the job.

Subroutine Development for Heat Source Model, $t_{8/5}$, Martensite Formation and Hardness

The conical heat source model has been developed and improved in several researches [9-11]. However, for this study, the heat source model is based on the works of Zhan et al. [12-14]. The conical heat source is represented by the mathematical model below.

$$Q_v = \frac{9Q_0}{\pi(1-e^{-3})} \cdot \frac{1}{(z_e-z_i)(r_e^2+r_e r_i+r_i^2)} \cdot \exp\left(-\frac{3r^2}{r_c^2}\right) \quad (1)$$

$$Q_0 = \eta P \quad (2)$$

$$r_c = f(z) = r_i + (r_e - r_i) \frac{(z-z_i)}{(z_e-z_i)} \quad (3)$$

Q_v represents the net heat flux and Q_0 represents the product of laser beam energy in (P) in watts and η the efficiency value. r_c in the equation represent the heat distribution coefficient as a function of z direction. r_e represent the maximum radius of the cone while r_i represent the minimum radius of the cone. Figure 6 below illustrates the conical heat source model.

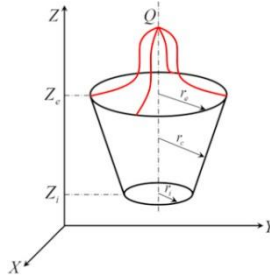


Figure 6: Illustration of Conical Heat Source Model

The dimensions of the heat source are defined as displayed in Table 3 below.

Table 3: Heat Source Dimension in FEM Simulation	
Heat Source Direction	Value
Max radius, r_e (mm)	1
Min radius, r_i (mm)	0.5
Depth, z_i (mm)	2

The developed subroutine *UWELDFLUX* for modelling the conical heat source model is shown below:

```

subroutine uweldflux (f,temflu,time)
real*8 f, temflu, time,
dimension temflu(*)
real x,y,z,pi,e,rc,ri,ze,zi,eff,p,rc, q1,q2,q3
pi=3.1415926, e=2.71828183, re=1, ri=0.5, ze=0, zi=-2,
p=1.4e6, eff=0.8
x=temflu(1), y=-temflu(2), z=temflu(3)
rc=ri+(re-ri)*(y-zi)/(ze-zi)
q1=9*p*(eff)/(pi*(1-1/(e*e*e)))
q2=1/((ze-zi)*(re**2+re*ri+ri**2))
q3=exp(-3*(x**2+z**2)/rc**2)
f=q1*q2*q3
    
```

In welding process, $t_{8/5}$ is the total time it takes for the welded material to cool from 800 to 500 degrees Celsius. While in most analysis, the temperature history is analysed from the start to the end, the $t_{8/5}$ is an approach that simplifies the process and is widely used in the welding industry.

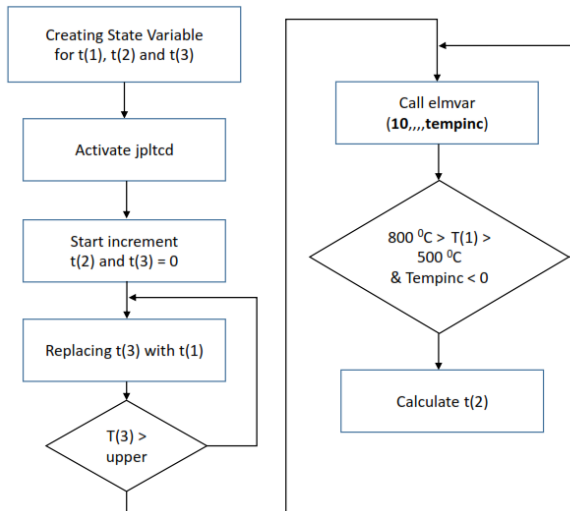


Figure 7: Algorithm for Calculating $t_{8/5}$

This is interval that most important microstructure change occurs, from austenite to other phase. In theory, if the $t_{8/5}$ is very short, more martensitic microstructure will form, while longer $t_{8/5}$ will result in formation

of mostly Ferrite and Pearlite. The calculation of $t_{8/5}$ is conducted by using self-developed subroutine and utility routine. The algorithm is illustrated in the flow chart below.

In MSC Marc/Mentat, information is stored in every increment for each node. To calculate the $t_{8/5}$, the nodal temperature data is extracted and used at each increment to analyse the $t_{8/5}$. State variables are data that is stored for each node, denoted by $t(*)$, where $t(1)$ is always the current temperature [15]. Since the $t_{8/5}$ is only the cooling time and not the heating time, an algorithm is written to only determine the decreasing section of the thermal cycle. The first argument of the algorithm is to begin calculation only when the peak temperature designated as $t(3)$ in the subroutine, reaches the upper limit, which is 800 degrees Celsius. Then a utility subroutine, *elmvar*, is used within the subroutine to extract temperature increments between each increment. A negative increment value will indicate that the nodes is cooling and the subroutine will begin calculating the $t_{8/5}$ or in this case $t(2)$. Calculation of $t_{8/5}$ is based on the use of fixed time steps. Meaning the subroutine will determine the total amount of increments taken for a node to cool from 800 to 500 degrees and then calculate $t_{8/5}$ by adding the fixed time interval between each two increments. The $t_{8/5}$ is stored independently for each node, allowing varying $t_{8/5}$ values throughout the workpiece. The developed subroutine *PLOTV* with utility routine *ELMVAR* for calculating $t_{8/5}$ is shown below:

```
subroutine plotv (jpltd)
real*8 s, sp, t, v, upper, lower, tempinc, timeinc
dimension t(*)
lower=500, upper=800, lastinc=300, timeinc=0.1
if(inc.eq.1) then t(2)=0 t(3)=0
if(t(1).gt.t(3)) then t(3)=t(1)
if(t(3).ge.upper) then call elmvar(10,m,nn,kcus,tempinc)
if(t(1).gt.lower.and.t(1).lt.upper.and.tempinc.lt.0) then
t(2)=t(2)+timeinc
v=t(2)
```

The phase transformation calculation is done using the Seyffarth Kassatkin model. Several other works to calculate phase transformation do exist, however the Seyffarth Kassatkin model is chosen as it utilises the $t_{8/5}$ approach. By using the *PLOTV* subroutine, the determined $t_{8/5}$ is used to calculate the Martensite phase prcentage as well as the hardness value of each nodes. The calculation is only done at the last increment because calculating the Martensite formation at each increment will hugely increase calculation time. The mathematical model is described with the equations below.

$$\ln t_m = -2.1 + 15.5 C + 0.84 Si + 0.96 Mn + 4.0 Al + 0.8 Cu + 0.77Cr + 0.7 Ni + 0.74 Mo + 0.3 V + 0.5 W - 13.5 C^2 \quad (4)$$

$$\ln T_M = 0.56 - 0.41 C + 0.1 Mn + 0.5 Cu + 0.14 Cr - 0.3 Mo + 2.7 Ti + 1.1 Nb + 1.7 C Mo \quad (5)$$

t_m is the starting time of formation for the Martensite phase, and T_M , represents the end time. In the equations above, C, Si, Mn, Cu, Cr, Ni, Mo, and W represents the percentage of each element in the material composition of the workpiece. t_A in the equation represents the $t_{8/5}$.

$$M = 100 \cdot \left[1 - \Phi \left(\frac{\ln t_A - \ln t_M}{\ln T_M} \right) \right] \quad (7)$$

$$\Phi(x) = \frac{1}{\sqrt{2\pi}} \int_{-\infty}^x e^{-\frac{1}{2}x^2} dt \quad (8)$$

M, represents the percentage distribution of Martensite. The percentage of Martensite is calculated using the cumulative distribution function (Φ) with the starting and ending time of formation.

The calculation of hardness (HV) is represented by the equation bellow:

$$HV = 323.6 - 114.6 \ln t_A + 11.33 \ln^2 t_A + 123.7 \ln t_A C_A - 1299 C - 79.11 Si - 120.7 Mn - 539 Cr + 79.22 Ni + 2830 Cr C + 620.8 C_A + 875.4 P_C \quad (9)$$

C_A and P_C are values used to represent the carbon equivalent:

$$C_A = C + \frac{Si}{24} + \frac{Mn}{6} + \frac{Cr}{5} + \frac{Ni}{40} + \frac{Mo}{4} + \frac{V}{14} \quad (10)$$

$$P_C = C + \frac{Si}{30} + \frac{Mn}{20} + \frac{Cr}{20} + \frac{Ni}{60} + \frac{Mo}{15} + \frac{V}{10} + \frac{Cu}{20} + \frac{B}{0.2} \quad (11)$$

The developed subroutine *PLOTV* with utility routine *ELMVAR* for calculating $t_{8/5}$ is shown below:

$$\begin{aligned} c=0.15, \quad si=0.22, \quad mn=0.41, \quad al=0.0005, \quad cu=0.15, \quad cr=0.06, \\ ni=0.06, \quad mo=0.036, \quad vl=0.026, \quad w=0.0, \quad ti=0.0, \quad nb=0.0 \\ lnstm=-2.1+15.5*c+0.84*si+0.96*mn+4.0*al+0.8*cu \\ +0.77*cr+0.7*ni+0.74*mo+0.3*vl+0.5*w \\ -13.5*c**2 \\ lnbtm=0.56-0.41*c+0.1*mn+0.5*cu+0.14*cr-0.3*mo \\ +2.7*ti+1.1*nb+1.7*c*mo \end{aligned}$$

$$\begin{aligned}
 ce &= c + si/24 + mn/6 + cr/5 + ni/40 + mo/4 + v1/14 \\
 pc &= c + si/30 + mn/20 + cr/20 + ni/60 + mo/15 + v1/10 + cu/20 \\
 argu &= (\text{dlog}(t(2)) - \ln stm) / \ln btm \\
 martensite &= 100.0 * (1.0 - \phi(\text{argu})) \\
 v &= \text{martensite} \\
 \\
 hv &= (323.6) - (114.6 * \text{dlog}(t(2))) + (11.33 * \text{dlog}(t(2)) * \text{dlog}(t(2))) \\
 &\quad + (123.7 * (\text{dlog}(t(2)) * cae) - \text{dlog}(t(2)) * cae) - (1299 * c) - \\
 &\quad (79.11 * si) - (120.7 * mn) - (539 * cr) + (79.22 * ni) + (2830 * cr * c) \\
 &\quad + (620.8 * cae) + (875.4 * pc) \\
 v &= hv
 \end{aligned}$$

To calculate the numerical integration of cumulative distribution function (ϕ) for calculating Martensite function, an algorithm using a simple trapezoidal integral function is developed and shown as below:

```

Real*8 Function phi (argu)
real*8 deltax,a,b,T,n,f,argu,i,xi,pi
a=-15.0, b=argu, n=30, T=0.0, pi = 3.1415927
deltax=(b-a)/n
do i=0,(n)
xi=a+i*deltax
if(i.eq.0.or.i.eq.(n))then T=T+exp(-0.5*xi**2)
else T=T+2.0*exp(-0.5*xi**2)
phi=1.0/sqrt(2.0*pi)*T*deltax/2.0
    
```

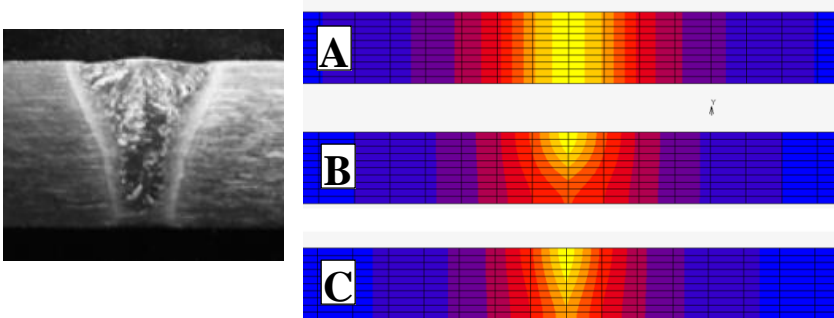


Figure 8: Comparison between Typical Laser Welding Macrograph [16] and Heat Source Models: Cylindrical (A), Double-Ellipsoid (B), Conical (C)

Result and Discussions

The simulation of was completed successfully with a total wall time of 3671 seconds. The cause of such a long calculation time is due to the implementation of subroutines. The conical heat source model has also been successfully implemented in the simulation using the *UWELDFLUX* subroutine. Observing the result from the post processing file, the difference between each type of heat source can clearly be seen. Figure 8 below shows the comparison between the three models and a macrograph of a deep penetration laser welding.

Since the $t_{8/5}$ time is calculated at the end of each increment, the calculation time increases drastically compared to a simulation done without the Martensite formation subroutine. The calculation time could be decreased using larger time steps, but this would give a less accurate $t_{8/5}$ time and thus resulting in a poor accuracy of Martensite percentage value. The number of nodes also determine the amount of calculation the solver has to do. While reducing the number of nodes used could improve wall time, this would reduce the accuracy of the analysis. A closer gap between nodes is needed, especially near the weld region to obtain a result with reasonable accuracy.

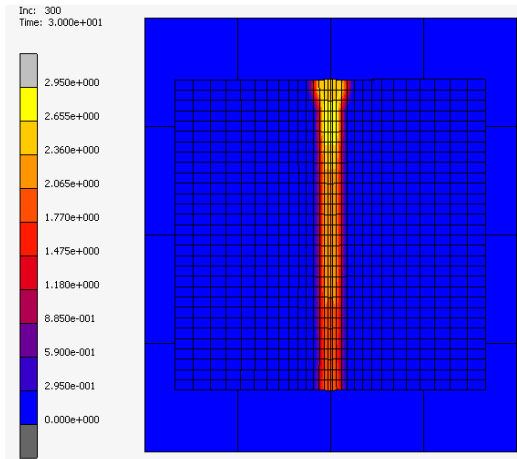


Figure 9: Predicted $t_{8/5}$ using Subroutine and Utility Routine

Figure 9 illustrates the total time taken for the nodes to cool from 800 to 500 degrees Celsius. The maximum $t_{8/5}$ is observed to be around 3 seconds in regions near the end of the weld path while it is observed that the region experiencing the fastest rate of cooling is at the start of the weldpath. This is

because at the start of the welding, the surrounding region is relatively cool making heat transfer faster.

Using the $t_{8/5}$ obtained, the Martensite formation is then calculated. The resulting Martensite distribution is illustrated in the figure 10 below.

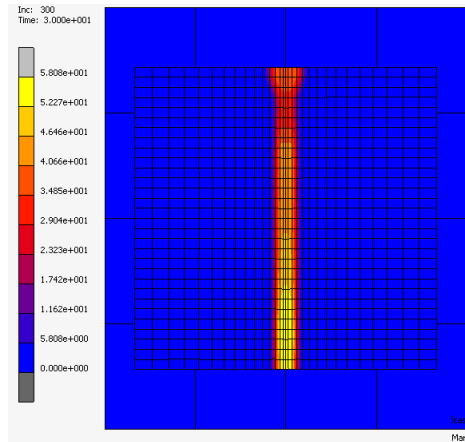


Figure 10: Distribution of Martensite Formation

It is observed that the Martensite formation is higher in regions that cool more rapidly. This shows the correlation between cooling time and the formation of Martensite. Table 4 below shows the percentage of Martensite in selected nodes compared to the calculated value based on the CCT diagram.

Table 4 : Percentage Distribution of Martensite

Node number	Simulation (%)	CCT (%)	Discrepancy (%)
4475	58.08	45 - 55	≈ 10
4484	47.22	35-45	≈ 15
4496	31.70	20-30	≈ 15

The simulation result of the Martensite formation shows good agreement with value predicted using the CCT diagram. However, the accuracy of both method is approximate at best. There are several factors that affects the accuracy of calculating the percentage numerically. The first being that the model is used for mild steel with a range of chemical compositions. Since the model only takes into account several chemical elements, the use of

elements beside those included in the numerical model may cause further inaccuracy.

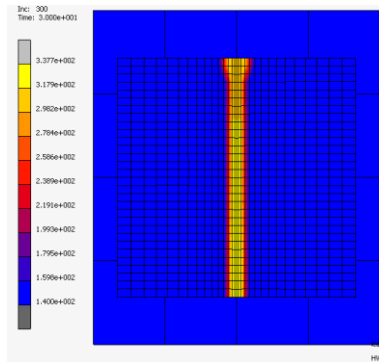


Figure 11: Hardness Value (HV30)

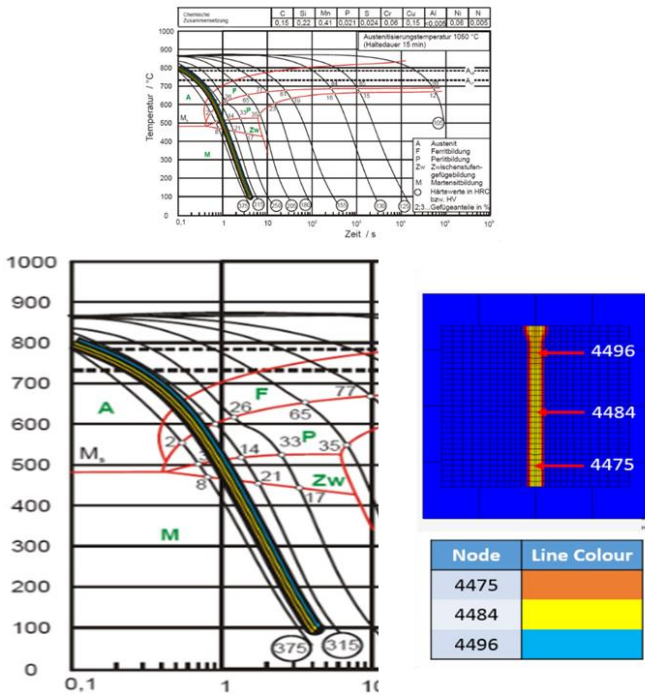


Figure 12: Result Analysis compared to CCT Analysis

The hardness values calculated are shown and compared to the CCT value in Table 5 below.

Table 5: Comparison between calculated and CCT values

Node number	Simulation (HV)	CCT (HV)
4475	330	
4484	325	330 - 350
4496	317	

Secondly, since the temperature is based on the $t_{8/5}$, the use of large elements in the FEA will make it even more inaccurate. This is because, the subroutine uses the temperature history of each nodes. The use of larger size elements will cause the nodes to be further away from each other and in turn cause huge difference in temperature, causing the calculation to be inaccurate. Thus, in order to have an acceptable result, a very fine mesh is required around the weldment. However, the use of fine mesh will drastically increase computation time.

From the $t_{8/5}$ the hardness value has been successfully calculated numerically. The hardness value correlates with the Martensite concentration, being higher at the start of the weld pass and lower at the end where the cooling rate is lower which can be seen in Figure 11.

The hardness value calculated are within the expected range of 375 to 315 obtained using the CCT method. The CCT analysis is illustrated below in Figure 12.

Conclusion

The prediction of phase transformation has been successfully achieved in MSC Marc/Mentat. To conclude this research, there are some crucial points that will be explained by following statements:

1. It is observed that only the cylindrical and conical heat source model could truly represent the deep penetration effects of the laser beam. However, the cylindrical model shows no loss of intensity with respect to depth, where in reality, the intensity of the heat decreases with penetration and thus will affect the temperature distribution of the Heat Affected Zone (HAZ).

2. With the use of mathematical models such as proposed by Seyffarth-Kassatkin, phase transformation could be simulated in FEA such as MSC Marc/Mentat with good accuracy
3. The heat source model plays an important role in temperature distribution of the HAZ and thus the best model must be used depending on the welding process chosen.
4. While the results are in good agreement with the CCT analysis, the Martensite phase distribution is still largely approximated. Further investigations and studies must be conducted to improve the accuracy and capability of FEA in simulating phase transformation.
5. The Martensite formation is calculated post process, meaning the actual mechanical effects of the Martensite formation is not considered in the structural analysis. Further work is needed to enable phase transformation to be considered in the analysis.
6. The selection of CCT diagram can affect the accuracy of simulation results as investigated in [17].
7. While increasing the amount of increment and using a finer mesh would greatly improve simulation accuracy, the calculation time is a limiting factor that needs to be considered in any simulation.

In conclusion, the simulation of welding processes is important not only to help reduce defects and scraps, but it is also important to achieve desired mechanical properties. Further investigation in the effects of welding in terms of phase transformation would prove to be beneficial for future studies.

Acknowledgement

The authors would like to express their gratitude to staff member of Welding Laboratory, Advanced Manufacturing Laboratory and Advanced Manufacturing Technology Excellence Centre at Faculty of Mechanical Engineering, Universiti Teknologi MARA (UiTM) for encouraging this research. The simulation was carried out at our partner university Chemnitz University of Technology in Germany under international research grant of DAAD (Ref. Nr.: 57347629). This research is also financially supported by Faculty of Mechanical Engineering UiTM Shah Alam and Geran Inisiatif Penyelidikan (GIP) from Phase 1/2016 with Project Code: 600-IRMI/GIP 5/3 (0019/2016).

References

- [1] Cary, Howard B; Helzer, Scott C. (2005). *Modern Welding Technology*. Upper Saddle River, New Jersey: Pearson Education. ISBN 0-13-113029-3.
- [2] Goldak, J., Chakravarti, A. and Bibby, M. (1984). A new finite element model for welding heat sources. *Metallurgical Transactions B*, 15(2), pp.299-305.
- [3] Wu, C., Hu, Q. and Gao, J. (2009). An adaptive heat source model for finite-element analysis of keyhole plasma arc welding. *Computational Materials Science*, 46(1), pp.167-172.
- [4] Tso-Liang Teng, Chin-Ping Fung, Peng-Hsiang Chang, and Wei-Chun Yang, Analysis of residual stresses and distortions in T-joint fillet welds, Chong Qing University 7 August 2011.
- [5] Xavier, C., Delgado Junior, H., Castro, J. and Ferreira, A. (2017). Numerical Predictions for the Thermal History, Microstructure and Hardness Distributions at the HAZ during Welding of Low Alloy Steels.
- [6] Patrick Mehmert (2002). Numerische Simulation des Metallschutzgasschweißens von Grobblechen aus un- und niedriglegiertem Feinkornbaustahl.
- [7] Jörg Hildebrand, J., Wudtke, I. and Werner, F. (2006). Möglichkeiten der Mathematischen Beschreibung Von Phasenumwandlungen Im Stahl Bei Schweiss- Und Wignachbehandlungsprozessen, 17th International Conference on the Applications of Computer Science and Mathematics in Architecture and Civil Engineering, Weimar in Germany.
- [8] Piekarska, W., Goszczynska, D. and Saturnus, Z. (2015). Application of analytical methods for predicting the structures of steel phase transformations in welded joints. *Journal of Applied Mathematics and Computational Mechanics*, 14(2), pp.61-72.
- [9] Sun, J., Liu, X., Tong, Y. and Deng, D. (2014). A comparative study on welding temperature fields, residual stress distributions and deformations induced by laser beam welding and CO₂ gas arc welding. *Materials & Design*, 63, pp.519-530.
- [10] Shanmugam, N., Buvanashakaran, G. and Sankaranarayananasamy, K. (2009). Experimental Investigation And Finite Element Simulation Of Laser Beam Welding Of Aisi 304 Stainless Steel Sheet. *Experimental Techniques*, 34(5), pp.25-36.

- [11] Mwema, F. (2017). Transient Thermal Modeling in Laser Welding of Metallic/Nonmetallic Joints Using SolidWorks Software. *International Journal of Nonferrous Metallurgy*, 06(01), pp.1-16.
- [12] Zhan, X., Liu, Y., Ou, W., Gu, C., & Wei, Y. (2015). The Numerical and Experimental Investigation of the Multi-layer Laser-MIG Hybrid Welding for Fe36Ni Invar Alloy. *Journal Of Materials Engineering And Performance*, 24(12), 4948-4957.
- [13] Zhan, X., Liu, Y., Ou, W., Gu, C., & Wei, Y. (2015). The Numerical and Experimental Investigation of the Multi-layer Laser-MIG Hybrid Welding for Fe36Ni Invar Alloy. *Journal Of Materials Engineering And Performance*, 24(12), 4948-4957.
- [14] Zhan, X., Li, Y., Ou, W., Yu, F., Chen, J., & Wei, Y. (2016). Comparison between hybrid laser-MIG welding and MIG welding for the invar36 alloy. *Optics & Laser Technology*, 85, 75-84.
- [15] MSC Team. *Marc Mentat 2015 User Guide Documentation Vol A to D*. MSC Software (2015).
- [16] Costa, A., Miranda, R., Quintino, L. and Yapp, D. (2007). Analysis of Beam Material Interaction in Welding of Titanium with Fiber Lasers. *Materials and Manufacturing Processes*, 22(7-8), pp.798-803.
- [17] Caron, J., Heinze, C., Schwenk, C., Rethmeier, M., Babu, S. S. and Lippoldt, J. (2010). Effect of Continuous Cooling Transformation Variations on Numerical Calculation of Welding-Induced Residual Stresses. *Welding Journal*, 89, pp. 152-160.